PrimEx Note 47

Single-Arm Compton Analysis

M. H. Wood

University of Massachusetts, Amherst

July 19, 2007

Abstract

The goal of the Primex experiment is a precise measurement of the π^0 radiative width. For this measurement to be believable, major components of the analysis such as yield extraction and incident photon flux must be checked systematically. Extracting cross sections for well-known processes like Compton scattering and pair production are possible cross-checks. In fact, dedicated runs were taken during the data collection for both of these processes. However, experimental conditions were changed to optimize these supporting runs. Moreover, the supporting runs give information before and after a period of π^0 production runs but do not show the data stability on the time scale of each run. Ideally, one would want to analyze a process from the π^0 production runs. This note will describe an analysis of Compton scattering reconstructed from the kinematics of the scattered photon. A comparison will be provided of this analysis technique on the π^0 production data and the dedicated Compton scattering runs.

Contents

List of Figures

List of Tables

1 Introduction

The Primex Experiment was conducted in the Fall of 2004 to measure with high precision the lifetime of the π^0 decaying into 2 photons. The device to detect the decay photons was the Hybrid Calorimeter (HyCal). The HyCal consists of blocks of $PbWO_4$ and Pb-Glass which collect the energy of the photons. A charged particle such as an electron will also deposit its energy in the calorimeter. Since the the HyCal will detect both photons as well as charged particles, a number of physical processes can be measured such as the π^0 with its two decay photons, Compton scattering with the scattered photon and recoil electron, and pair production where the photon converts to an electron-positron pair. The well-known electromagnetic interactions of Compton scattering and pair production could be employed as systematic checks on the quality and stability of the π^0 data.

In order to extract the π^0 lifetime with the Primex data, one needs to determine the absolute cross section of the Primakoff reaction. The major components of this cross section are the two-photon yield, number of incident photons, the acceptance, and number of target centers. The number of target atoms was obtained by Ref. [1] and will not be discussed here. Each of the three remaining parts are checked by determining the cross section from the supporting reactions (Compton scattering and pair production). The most direct comparison comes with the number of incident photons since that value is supplied independently of each analysis. With respect to the yields and acceptances, the same software machinery is used even though there are different cuts and event selection.

The ideal situation would be to produce Compton scattering and pair production cross sections from the same runs with the π^0 production data. Within a short time interval (i.e. one run), the quality of the data could be monitored. Unfortunately, the running conditions could not be optimized for all three reactions. The Pair Spectrometer (PS), which is an online monitor of the relative photon flux, contains a large dipole magnet which sweeps out the electrons in the horizontal plane. Therefore, dedicated calibration runs were taken where the current of the PS magnet was set to zero for Compton scattering runs or reduced for the pair production runs. In order to optimize these calibration runs, the HyCal-total-sum trigger threshold was reduced 2 GeV to 500 MeV. With the calibration runs conducted separately from the π^0 production runs, they provide limited confidence as monitors of beam and HyCal stability. If a change occurred in the experimental conditions, one would not be aware of it until the calibration run at the end of the production data period. In this scenario, large portions of the data would need to be discarded. What is needed is a reaction channel which could be analyzed from the π^0 production data.

One possible analysis is Compton scattering reconstructed from the scattered photon. If a photon scattered off of an atomic electron from the target during the production run, the electron would be swept away by the PS magnet, and the scattered photon would travel to the calorimeter unaffected. The HyCal detector would provide the energy and polar angle of the scattered photon. The Veto Counters (VC) would discriminate the particle as a photon and clean up the data sample. Finally, the Compton scattering cross section is large enough to provide a statistically-significant result.

The yield extraction depends on three observables: the scattered photon energy ($E_{cluster}$, the incident photon energy (E'_γ), and the scattered photon polar angle (θ). The incident photon energy is provided by the photon tagger. The energy and angle of the scattered photon is obtained from the HyCal. The quantities E'_γ and θ are used to calculate the expected Compton scattering energy by inserting them into the following equation:

$$E_\gamma = E'_\gamma \left[\frac{m_e}{m_e + E'_i(1 - \cos\theta)} \right], \tag{1}$$

where m_e is the mass of the electron. The ratio, R, given by the equation

$$R = E_{cluster}/E_\gamma, \tag{2}$$

will have a peak at 1 for Compton scattering events. Everything else in the R distribution will be background.

The single-arm Compton analysis will be checked by analyzing the data from dedicated Compton scattering runs. The VC should discriminate between the scattered electron and photon in each event. The same analysis software will be applied to the dedicated Compton scattering run as with the π^0 production run. After acceptance corrections, the extracted cross sections should agree within errors.

This note will discuss the event selection criteria (Sec. 2), trigger inefficiency (Sec. 6), acceptance issues (Sec. 4), and preliminary results (Sec. 5). Some suggestions for the next Primex experiment with given in the conclusions section (Sec. 8).

2 Event Selection

The event selection for the single-arm Compton analysis is different from the other reaction analyses in that it is the only one to employ a single cluster in HyCal. All of the other analyses require two clusters. This section will describe the cuts which were applied to select a single cluster and the most-likely tagged photon.

2.1 Single Cluster Cuts

In any arbitrary event, they could be several clusters which register in the calorimeter. The first task in this analysis was to pick the most-likely cluster to have originated from Compton scattering. Fig 1 shows the number of clusters in a given event. From these plots, there are a large number of single cluster events which would be thrown out by the π^0 analyses. However, these are are prime candidates for this analysis. Events were kept if there was at least one cluster per event. Multiple cluster events were also kept since there could be a background photon in the event with the true Compton scattered photon. In these multiple cluster events, the scattered photon candidate was chosen using a likelihood procedure. Fig. 2 shows preliminary ratios of cluster energy to expected Compton energy with different numbers of clusters per event for a π^0 production run with the ^{12}C target. A peak at 1.0 is clearly seen for events with two clusters which justifies including multiple-cluster events. The other interesting observation is that the background shapes are different for the different event types. The higher number of clusters per event creates background which is smaller in the value of the energy ratio.

Other standard cuts were applied in the cluster selection. Any cluster with a deposited energy less than 0.5 GeV was discarded. This cluster energy cut was used in all other Primex analyses to reduce accidental background. A position reconstruction cut of $x \geq 4.5$ cm and $y \geq 4.5$ cm was applied to reject clusters near the beamline hole in the calorimeter. For this analysis, the cluster should be identified as a photon so a VC status cut was applied where the veto flag in the HYCALCLUSTER bank was less than zero. Finally, the event had to have a valid,

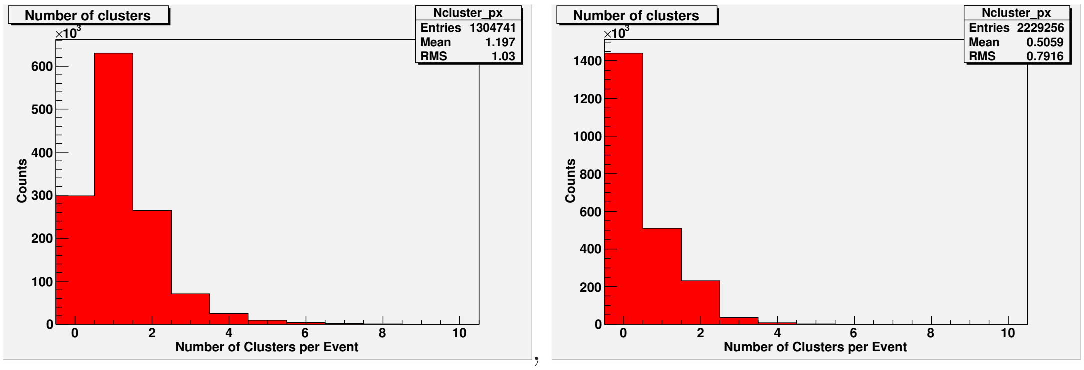

Figure 1: Plot of the number of clusters per event from a π^0 production run (left) and a Compton scattering run (right).

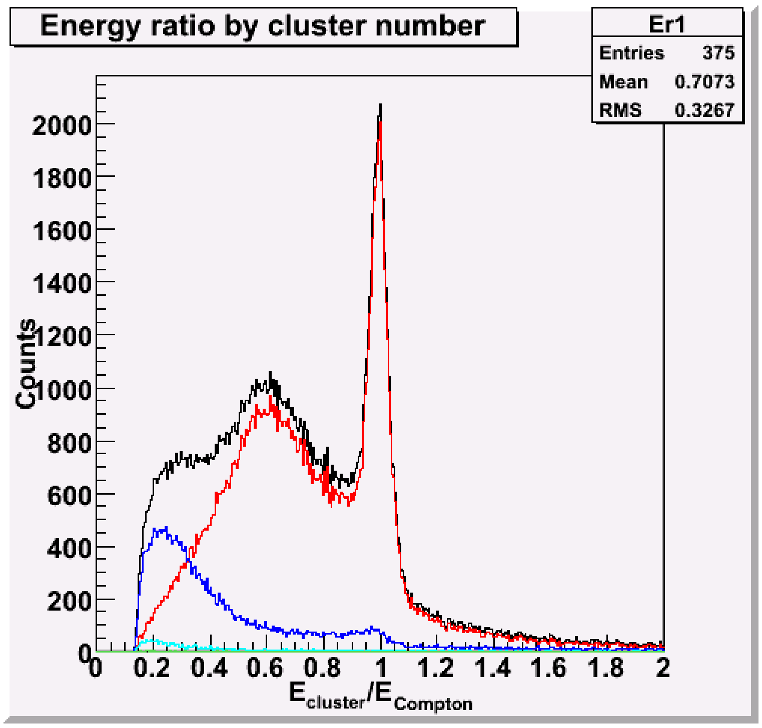

Figure 2: Plot of the energy ratio R for different numbers of clusters per event where black is all events, red is single-cluster events, blue is two-cluster events, and cyan is three-cluster events. This data is taken from run 5003, a π^0 production run.

tagged photon. The tagged photon candidates were selected if the bit id in the TRIGPHOTON bank was set to 2. A summary of the cuts are listed in Table 1.

Table 1: Summary of event selection cuts.

Cut	Description
Cluster energy	$E_{cluster} \geq 0.5$ GeV
Cluster x-position	$x \geq 4.5$ cm
Cluster y-position	$y \geq 4.5$ cm
Veto status	HYCALCLUSTER.veto < 0
Tagged photon	TRIGPHOTON.id $= 2$

2.2 Likelihood Analysis

After the cluster cuts have been applied, the remaining events can still have more that one photon in HyCal as well as numerous tagged incident photons. To reduce the scattered and incident photon candidates to a single pair, a likelihood analysis is conducted. Two probabilities are calculated and combined to form the likelihood distribution. The first probability is the timing difference between the tagged photon and the HyCal total sum. Fig. 3 is an example of such a timing distribution. The timing difference spectrum was fit with a Gaussian for the peak and a linear function for the background. The fit parameters are a mean of -0.18 s and a sigma of 2.25 s. These parameters are used to calculate the timing probability on an event-by-event basis. The second probability is the energy ratio R. Fig. 4 shows a typical R distribution for a π^0 production run. This distribution was fit with a Gaussian and a third-order polynomial background shape. The mean and sigma of the peak are found to be 1.02 and 0.04, respectively. With the parameters for both probability functions in hand, the likelihood is the product of the probabilities for each pair of candidates. Figs. 5 and 6 show the probability distributions for the timing difference and R, respectively. Fig. 7 is a histogram of the total likelihood distribution.

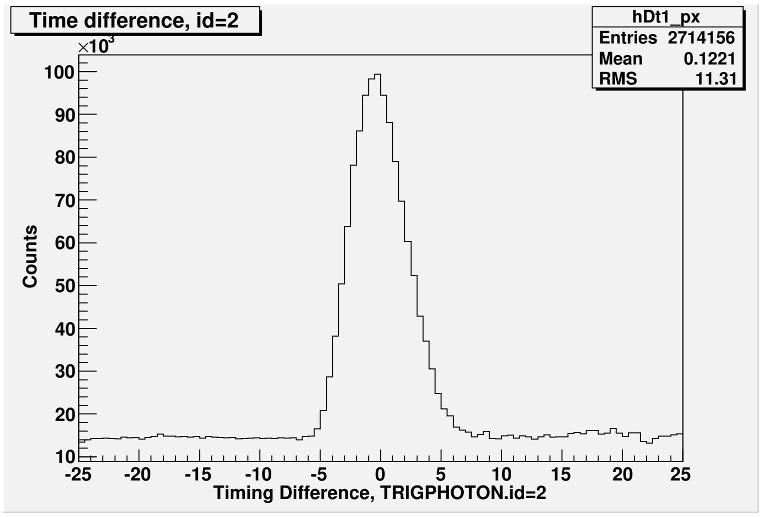

Figure 3: A typical timing-difference spectrum for a π^0 production run with no event selection applied except for a valid tagged photon. A fit to this distribution provided the parameters for the probability density for the Δt.

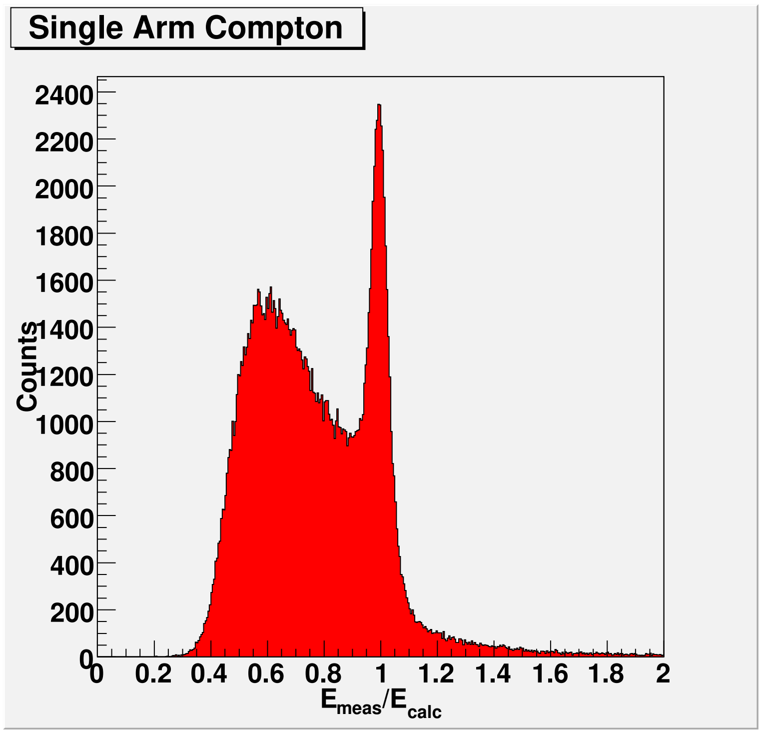

Figure 4: A typical energy ratio spectrum for a π^0 production run with no event selection applied except for a valid tagged photon. A fit to this distribution provided the parameters for the probability density for R.

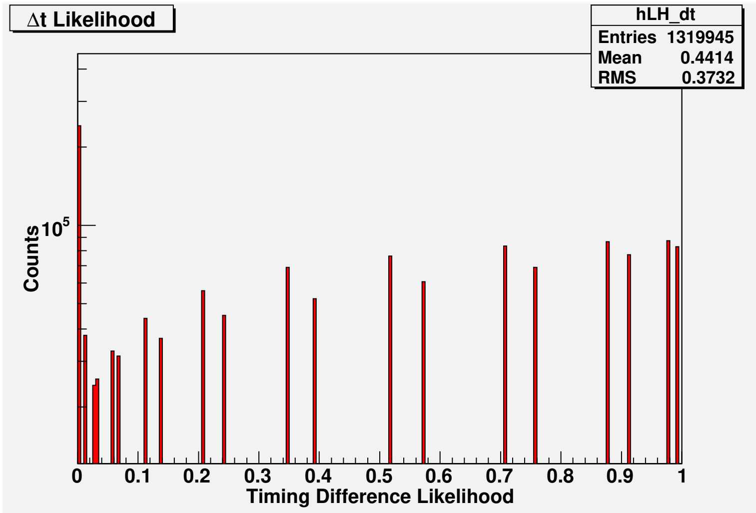

Figure 5: The likelihood distribution for the timing difference.

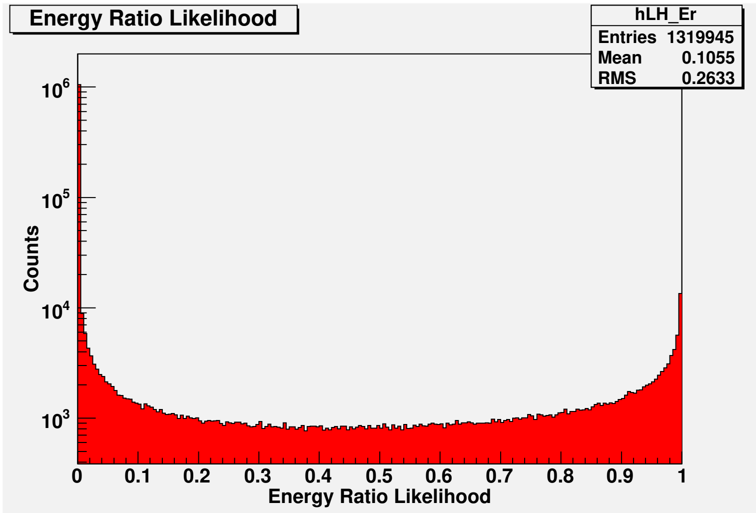

Figure 6: The likelihood distribution for the energy ratio.

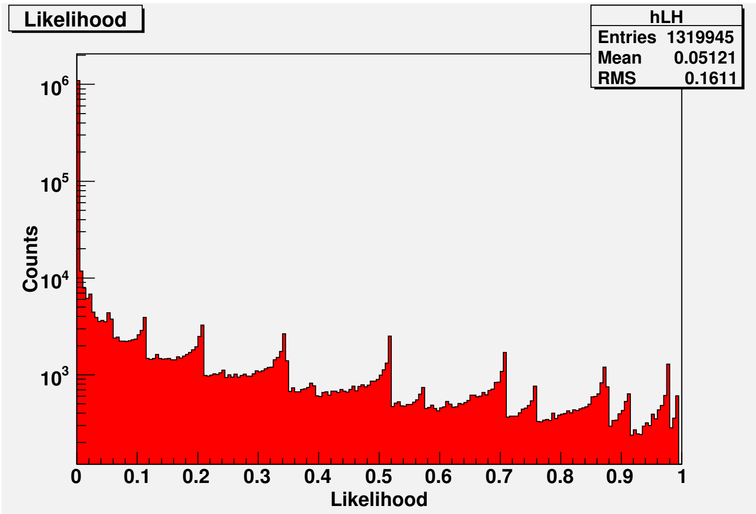

Figure 7: The total likelihood distribution. The saw-tooth pattern is comes from the timing difference likelihood which has the beam timing-structure in it.

2.3 Angular Range

In order to extract the yield reliably, an angular range is chosen to maximize the signal and minimize the background in the R distribution. The energy ratio is plotted in angular bins of 0.1°. The background is greatest at low polar angles and diminishes as the angle increases (see Fig. 8). The peak survives out to $\theta = 1.7°$; however, the spectra are dominated by background. The angular range for the cross section determination is set at $0.5° \leq \theta \leq 0.9°$ due to trigger inefficiencies which will be discussed later.

The R distributions for the dedicated Compton scattering runs have different background shapes. Fig. 9 shows the R spectra divided into 0.1° bins for a Compton scattering run. The background is much smaller than in the case of the $\pi^{)}$ production run. Also, the Compton scattering run extends to a much wider angular range.

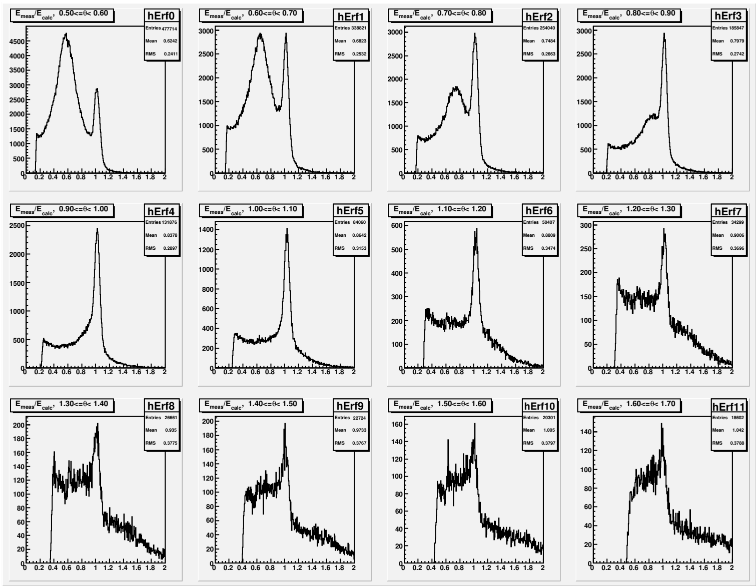

Figure 8: The energy ratio in angular bins of 0.1° for run 5003, a π^0 production run. The specific angular range for each plot is labeled in the histogram title box.

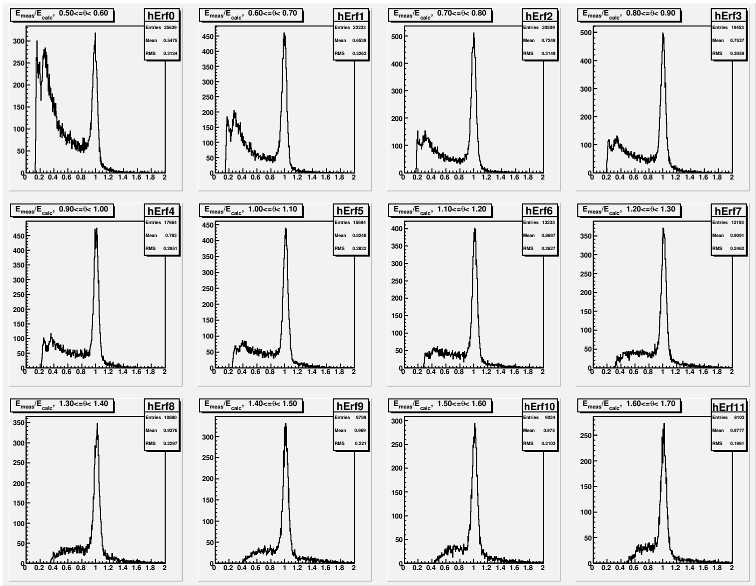

Figure 9: The energy ratio in angular bins of 0.1° for run 5150, a dedicated Compton scattering run. The specific angular range for each plot is labeled in the histogram title box.

3 Yield Extraction

The yields are extracted by fitting the peak of the R distribution with a skewed-Gaussian function and a polynomial background shape. For both types of runs($\pi^)$ production and Compton scattering), the same functional forms are employed; however, the fit ranges are changed for optimization. In order to approximate the energy dependence of the cross section, the yields are divided in bins by T-counter number. For the π^0 production runs, the first eleven T-counters were turned on. During the Compton scattering runs, other T-counters were activated but are neglected in this analysis in order to compare both types of runs.

Figs. 10 and 11 show the fits to the production and Compton scattering runs, respectively. The top, left plot in each figure is the total statistics from all T-counters. The R distributions for the Compton scattering runs is much cleaner than in the case of the production run. For the π^0 production run, there is a large background peak around 0.5 which is almost of equal height with the Compton scattering peak at 1.0. Three different background shapes are employed in order to determine which would provide the most stable background subtraction. The three background functions are third-order polynomial, second-order polynomial, and a Gaussian. The fit-range is varied on the left-side for each background shape in order to guage stability. For the 2^{nd}-order polynomial, the fit range is attempted from 0.6, 0.7, and 0.8 to 1.2. For the 3^{rd}-order polynomial, the fit range is attempted from 0.6, 0.7, and 0.8 to 1.2. Finally, For the Gaussian, the fit range is attempted from 0.4, 0.5, and 0.6 to 1.2. In each case, the chi^2 per degree of freedom are good with all fits below 2.0. Figs. 12, 13, and 14 are plots of the chi^2 per degree of freedom for each T-counter with the different background forms and different fit-ranges. The fits with the 2^{nd}-order polynomial show some fluctuations in the chi^2 per degree of freedom when the fit range is varied a small amount. The other background shapes are much more stable. A comparison of the cross sections with the different background subtractions will be shown in Sec. 5. The 3^{rd}-order polynomial is chosen for the background form since it can be applied to both production and Compton scattering analyses.

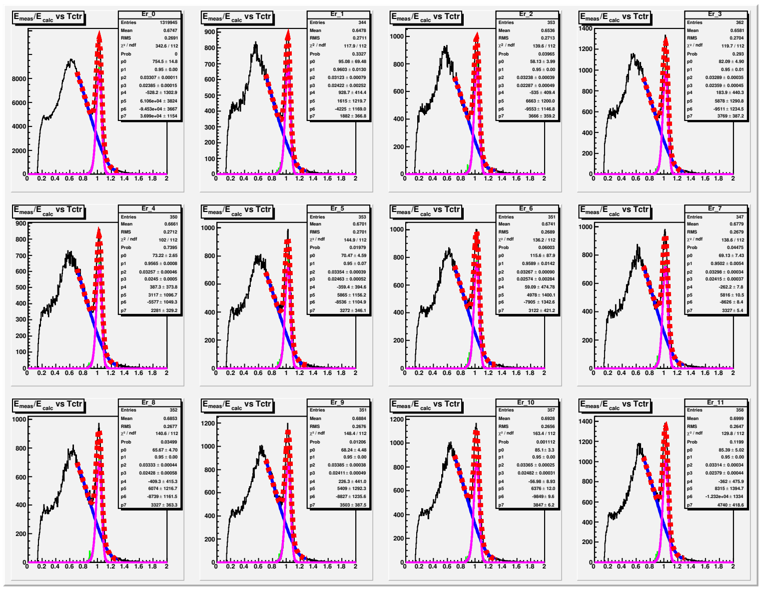

Figure 10: Fits to the energy ratio for run 5003, a π^0 production run, with a skewed gaussian for the peak and a third-order polynomial for the background. The blue line is the background shape, and the magenta histogram is the subtracted signal. The red, dashed line is the combined peak and background functions.

3.1 Empty Target Analysis

For the π^0 production runs, the yield determimation would be easier and have a smaller systematic error if the background in the R distribution could be reduced. A means to reduce background is to analyze the empty target runs. The same software used for the data with the carbon target in the beam has been applied to the data without the target. The idea is that the background in the R distribution is originating from the accidental photon interacting with the beamline components. Table 2 lists the runs with the target out of the beam. Fig. 15 shows the R distribution for run 5115. This distribution needs to be scaled before it can be subtracted from the π^0 production data. This scaling can be done properly by using the photon flux from each type of run. However, as a quick and dirty test to see the effect of the empty target data, the empty target R distribution is scaled manually to match

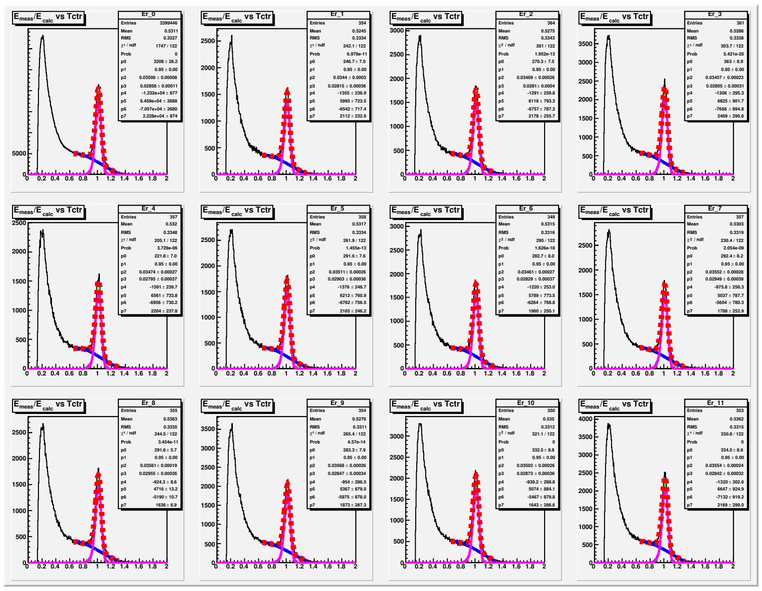

Figure 11: Fits to the energy ratio for a group of Compton scattering runs with a skewed gaussian for the peak and a third-order polynomial for the background. The blue line is the background shape, and the magenta histogram is the subtracted signal. The red, dashed line is the combined peak and background functions.

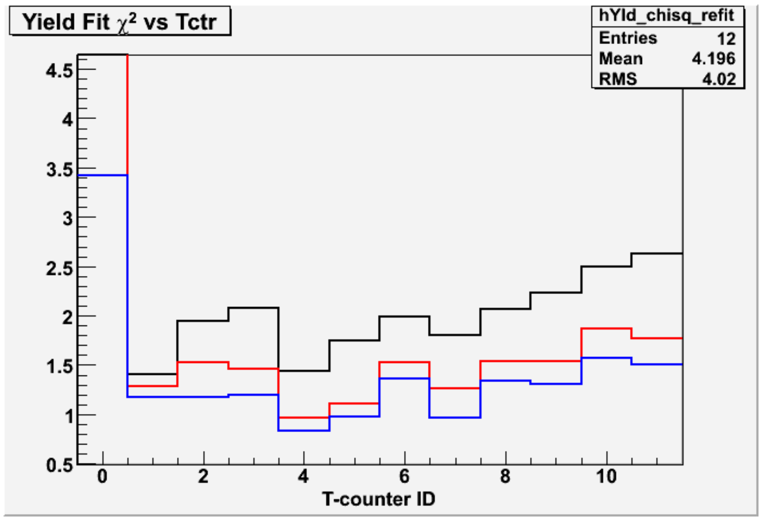

Figure 12: The χ^2_{ndf} per T-counter for fits to the π^0 production run 5003. The fits contain a skewed-gaussian for the signal and a 2^{nd}-order polynomial for the background. The different colors are for various fit ranges of the background: black($0.7 \leq R \leq 1.2$), red($0.75 \leq R \leq 1.2$), and blue($0.8 \leq R \leq 1.2$)

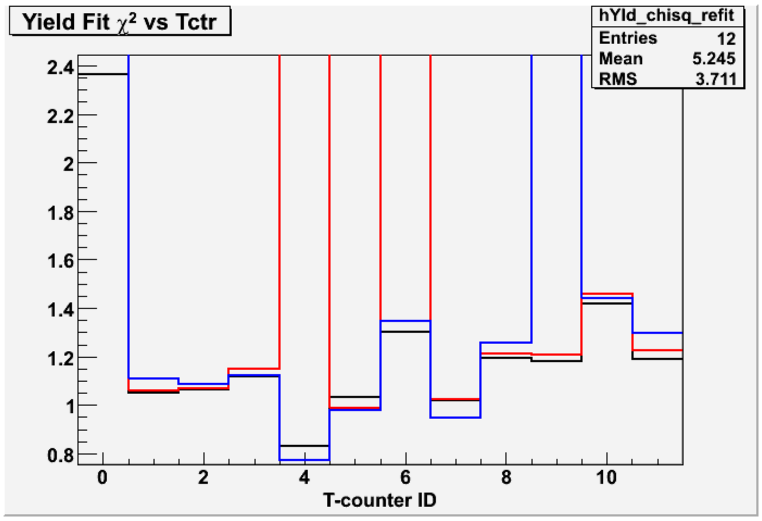

Figure 13: The χ^2_{ndf} per T-counter for fits to the π^0 production run 5003. The fits contain a skewed-gaussian for the signal and a 3^{rd}-order polynomial for the background. The different colors are for various fit ranges of the background: black($0.7 \leq R \leq 1.2$), red($0.75 \leq R \leq 1.2$), and blue($0.8 \leq R \leq 1.2$)

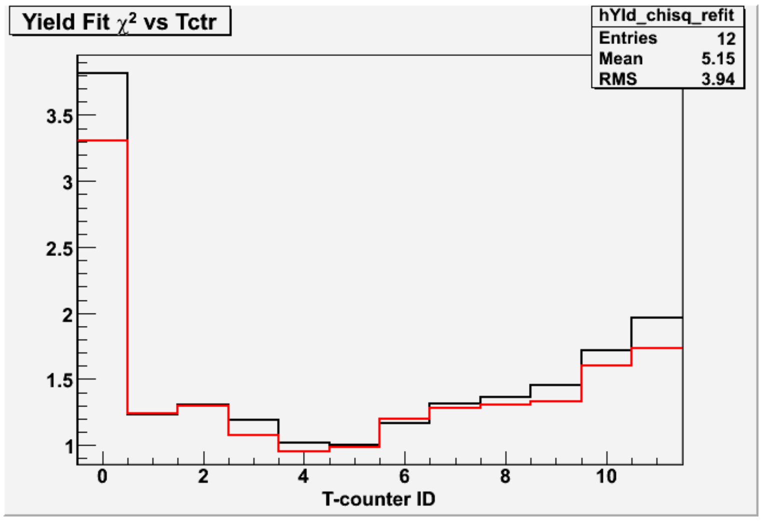

Figure 14: The χ^2_{ndf} per T-counter for fits to the π^0 production run 5003. The fits contain a skewed-gaussian for the signal and another gaussian function for the background. The different colors are for various fit ranges of the background: black($0.45 \leq R \leq 1.2$), and red($0.55 \leq R \leq 1.2$)

Table 2: Run numbers for empty target data.

Run Numbers	Data Type
5115-5134	π^0 production
5158	Compton scattering
5319	Pair production

the background in the distributions from both runs (see Fig. 16). In this figure, the shape of the backgrounds match quite well for $R \leq 0.5$. Fig. 16 also shows the background-subtracted R distribution. Unfortunately, the low R background is not a flat distribution, and the task of fitting the background is even more difficult than before the background subtraction. There remains a source of background which is not accounted for with the empty target data. The empty target data were not employed in this analysis.

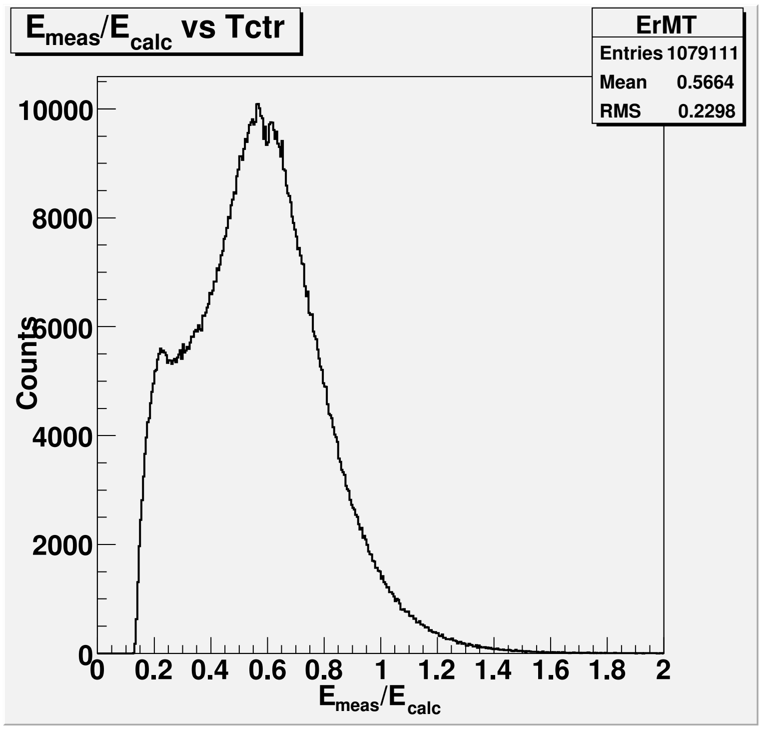

Figure 15: The energy ratio from empty target run 5115.

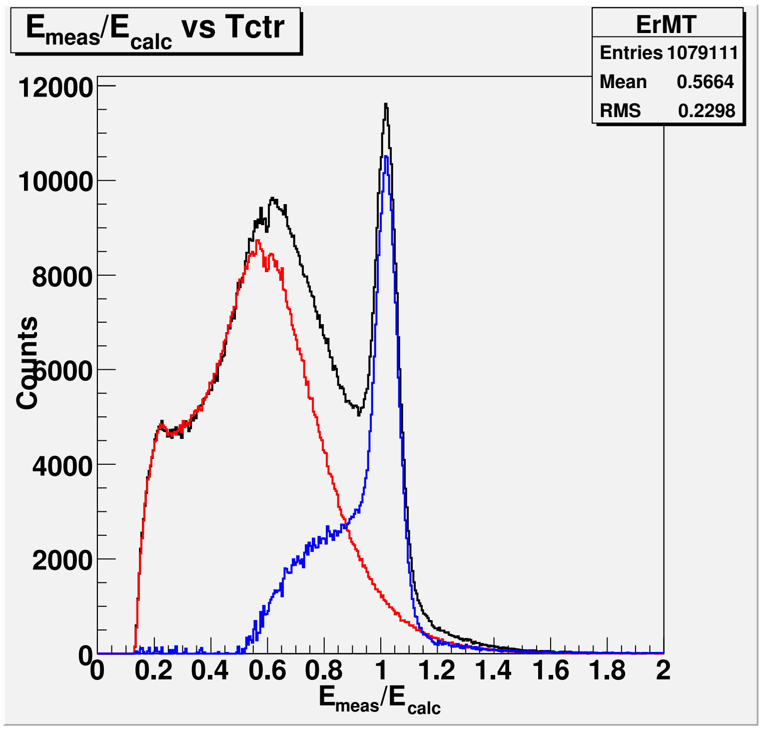

Figure 16: The energy ratio from empty target run 5115 (red) scalled to match the low-end of the distribution from a π^0 production run (black). The blue histogram is after the subtraction of the empty target data.

4 Acceptance

In order to produce an absolute cross section, the normalized yields must be adjusted for the detector acceptance and efficiency. At the current state of this analysis, a global acceptance has been calculated. If a more mature analysis is conducted in the future, the acceptance by T-counter and precise detector efficiencies should be determined. This analysis is a first pass at the single-arm Compton cross section and will be considered a success if the agreement with the theory is within 5%.

The global acceptance is determined in a standard way. The events are generated with the `GCOMP` routine in `GEANT`. Next, the generated particles are tracked from the target geometry through the other beamline components until they stop in the HyCal materials or miss the detector entirely. The generator and detector simulation are contained in the `primsim` software package. The initial parameters in ffread file for `primsim` are listed in Table 3.

The output from `primsim` is `MCPART` and `MCDEPOSITED` banks (monte-carlo banks) which are written in coda format. The `MCPART` bank contains the list of generated, intermediate, and final particles with various physical quantities such as energy, momentum, polar angle, azimuthal angle, and creation vertex. The `MCPART` bank is used to create the generated or thrown distributions. The `MCDEPOSITED` bank contains information on the energy deposited in each detector system (HyCal, Veto, PS, etc.). This information is the input to the next software package (`psim_digitize`).

The package `psim_digitize` has two functions: convert the energy information in the `MCDEPOSITED` bank into raw banks like HYCAL, VETOA, and VETOT which contain ADC and TDC information. With the digitized, raw banks, the output of `psim_digitize` can be the input in standard Primex analysis software. The second function of `psim_digitize` is to apply the empirical detector resolutions so that the simulated events match the actual data.

Since two types of runs are analyzed (π^0 production and Compton scattering), the primsim software has been run twice, with and without the magnetic field from the PS magnet. The global acceptance for the production and Compton scattering

Table 3: Values used in the `ffread.in` for the single-arm Compton simulations for π^0 production settings. For a dedicated Compton scattering run, the PSMG variable is set to 0.0.

Variable Name	Value
TRIG	1000000
DEBUG	0 0 0
SWIT	0 1 0 0 0 0 0 0 0 0
CUTS	5*1.E-2
EGFR	5.734 0.200 0.9500
RUNG	5000 1
RNDM	553497274 1937530786
TGTN	1
SHUT	0
PSMG	17.0
HCUT	0.0
GENR	4
PRVW	45.0 45.0 0.0 16.875 16.875 0.03125 0.03125

runs is calculated to be 11% and 11%, respectively, in the angular range from 0.5° to 1.3°. Table 4 lists the acceptances for different angular ranges. It should be noted that the acceptances are approximately the same for each run type.

Table 4: Acceptance for detecting the scattered photon in the range from 0.5° to θ_{max}. The two run types are π^0 production (with B_{PS}) and Compton scattering (without B_{PS}).

θ_{max} (°)	Acceptance (π^0 run)	Acceptance (Compton run)
0.6	0.017	0.016
0.7	0.033	0.032
0.8	0.048	0.047
0.9	0.063	0.062
1.0	0.077	0.076
1.1	0.090	0.089
1.2	0.102	0.101
1.3	0.117	0.112

5 Results

The yield, acceptance, number of incident beam photons, and number of target electrons can be combined to form the cross section. The cross section is determined in T-counter bins for the first eleven T-counters. Fig. 17 shows the comparison of cross sections determined for the Compton scattering runs and a π^0 production run. Also, plotted in the figure is the cross section calculated with the Klein-

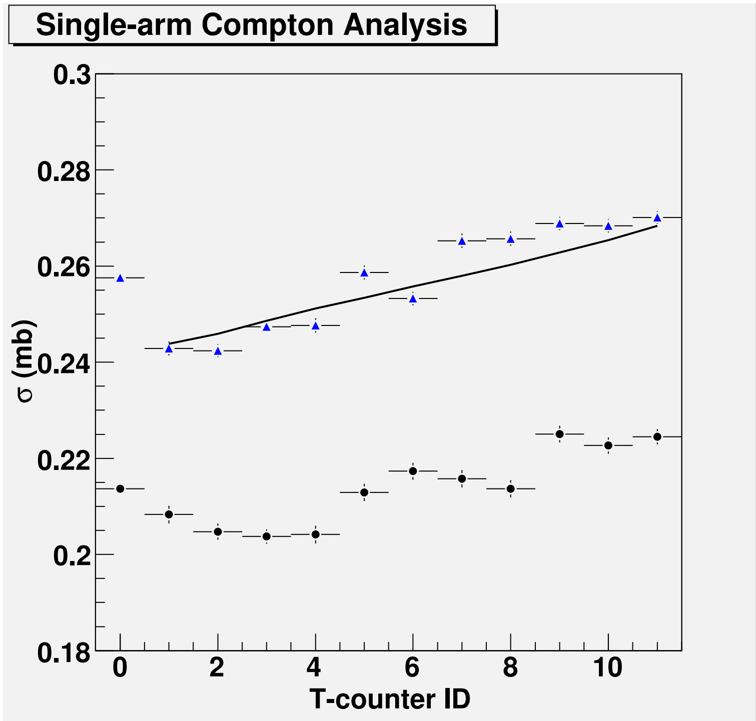

Figure 17: A comparison of the total cross section from a π^0 production run (black circles), some Compton scattering runs (blue triangles), and a Klein-Nishina calculation (black line).

Nishina equation. To calculate the total theoretical cross section, one starts with the differential form given as

$$\frac{d\sigma}{d\Omega_\gamma} = \frac{r_e^2}{2}\left\{P(E,\theta) - [P(E,\theta)sin(\theta)]^2 + [P(E,\theta)]^3\right\}, \tag{3}$$

where r_e is the classical electron radius and $P(E,\theta)$ is

$$P(E,\theta) = \frac{1}{1 + \frac{E'_\gamma}{m_e}[1 - cos(\theta)]}. \tag{4}$$

Next, Eq. 3 is integrated over the angular range from 0.5° to 0.9° for the scattered photon

$$\sigma = \int_{0.5^\circ}^{0.9^\circ} \frac{d\sigma}{d\Omega_\gamma} d\Omega \tag{5}$$

To make a proper comparison between the theory and the experimental data, the theoretical results have been adjusted with the detector acceptance for this polar angular range.

The cross section from the dedicated Compton scattering runs is in good agreement with the Klein-Nishina prediction. This result is encouraging since an agreement within 5% between the double-arm Compton result [2] and Klein-Nishina calculations. The single-arm result of the π^0 production run disagrees with the theoretical calculation and the result from the Compton scattering run by 20%.

5.1 Raising the θ_{min} Cutoff

In Sec. 2.3, the R distribution is studied in θ bins of 0.1°. It was determined that the background is dominant at lower values of θ consistent with the background originating from the beamline. An idea is to raise the θ_{min} cut in order to decrease the background substantially while decreasing the signal minimally. Fig. 18 shows the effect of raising the θ_{min} cut while fixing $\theta_{max} = 0.9°$. The background is greatly reduced by raising the θ_{min} cut; however, the peak of the background is moving up closer to the signal peak. At some point, it is not advantageous to raise the θ_{min} cut because background subtraction becomes less certain. One would like to have a background which is modeled well which is not the case when the background peaks under the signal. In the next section, a comparison will be made between cross sections determined with the angular ranges $0.5° \leq \theta \leq 0.9°$ and $0.6° \leq \theta \leq 0.9°$. It will be shown that changing the angular acceptance does not increase the agreement between the experimental data and the Klein-Nishina calculation.

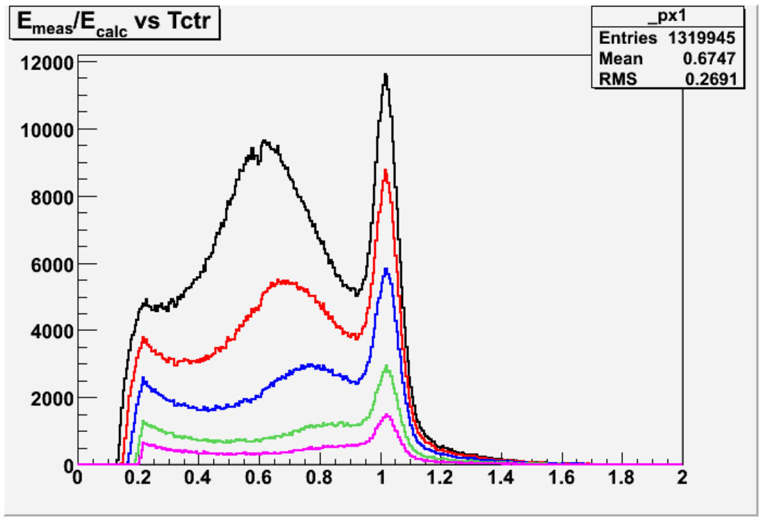

Figure 18: A comparison of the energy ratio for various θ_{min} cutoffs. The value of θ_{min} for each line is $0.5°$ (black), $0.6°$ (red), $0.7°$ (blue), $0.8°$ (green), and $0.85°$ (magenta). The data are from a π^0 production run.

5.2 Effect of Background Fits

As discussed in Sec. 3, different functional forms have been tested in the yield extraction. These different functional forms have been studied to improve the agreement between the π^0 production result and the other results. Fig. 19 shows a comparison of the cross sections determined by various background forms. None of the yields obtained by the different background forms improved the agreement between the experimental data and the theory. Moreover, this comparison indicates that there is a preliminary systematic uncertainty in the background subtraction on the order of 10%.

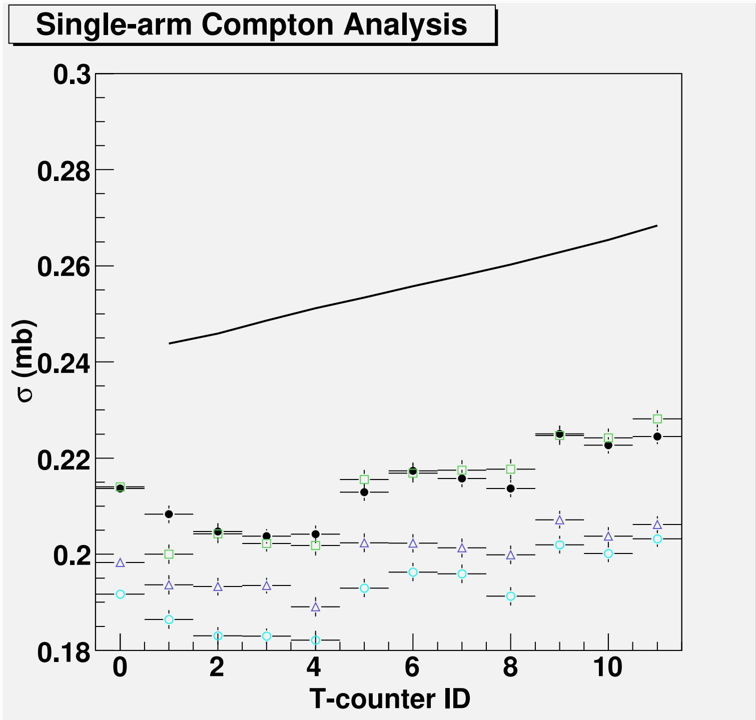

Figure 19: A comparison of the total cross section from a π^0 production run. The black circles are determined by 3^{rd} order polynomial fits to the background with the angular range from $0.5°$ to $0.9°$. All other data points are analyzed with an angular range from $0.6°$ to $0.9°$. The other data points are determined with different background forms: 3^{rd} order polynomial (cyan open circles), 2^{nd} order polynomial (green squares), and a Gaussian (blue triangles). The black line is the Klein-Nishina calculation.

6 Trigger Studies

The disagreement between the results from the π^0 production run and the Compton scattering run appears to come from a trigger inefficiency. A hardware, trigger threshold was applied on the total energy summed over all HyCal elements during the data collection. This trigger threshold was changed to optimize event collection for each run type. For the π^0 production runs, the threshold was set at 2 GeV. For the Compton scattering runs, the value was lowered to 0.5 GeV. The effect of the trigger threshold can be seen in Fig. 20 where the R distribution is plotted versus the cluster energy. The plot on the left is for a π^0 production run which contains mostly high-energy photons. For the Compton scattering run on the right, low-energy photons are preferred. It is clear that two different samples of Compton-scattered photons are being analyzed.

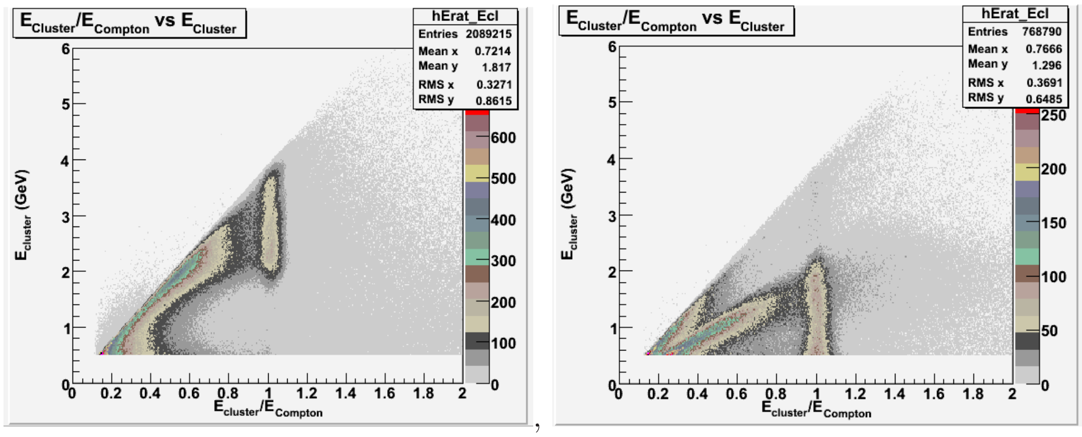

Figure 20: Plot of R versus $E_{cluster}$ for a π^0 production run (left) and a Compton scattering run (right). The hardware trigger threshold is clear for each run type that the π^0 production data prefer high-energy clusters while the Compton scattering data prefer low-energy photons.

Since the energy and the angle of the scattered photon are correlated, the θ_{max} cut can be lowered to select the higher-energy photons. The idea is to limit the phase space to a region where the kinematics match for both run types. In this region, the trigger efficiency should be the same for both runs. Fig. 21 is a plot of the normalized yield from a π^0 production run for various cuts on θ_{max}. The yield has been normalized to the number of incident photons and detector acceptance. For every point, θ_{min} has been set equal to $0.5°$. This study shows a plateau for yields at $0.9° \leq \theta max$ which is the reason it has been chosen as the cutoff in the analysis. The deviation of the point at $0.6°$ is attributed to the background subtraction since the background is the greatest at this setting.

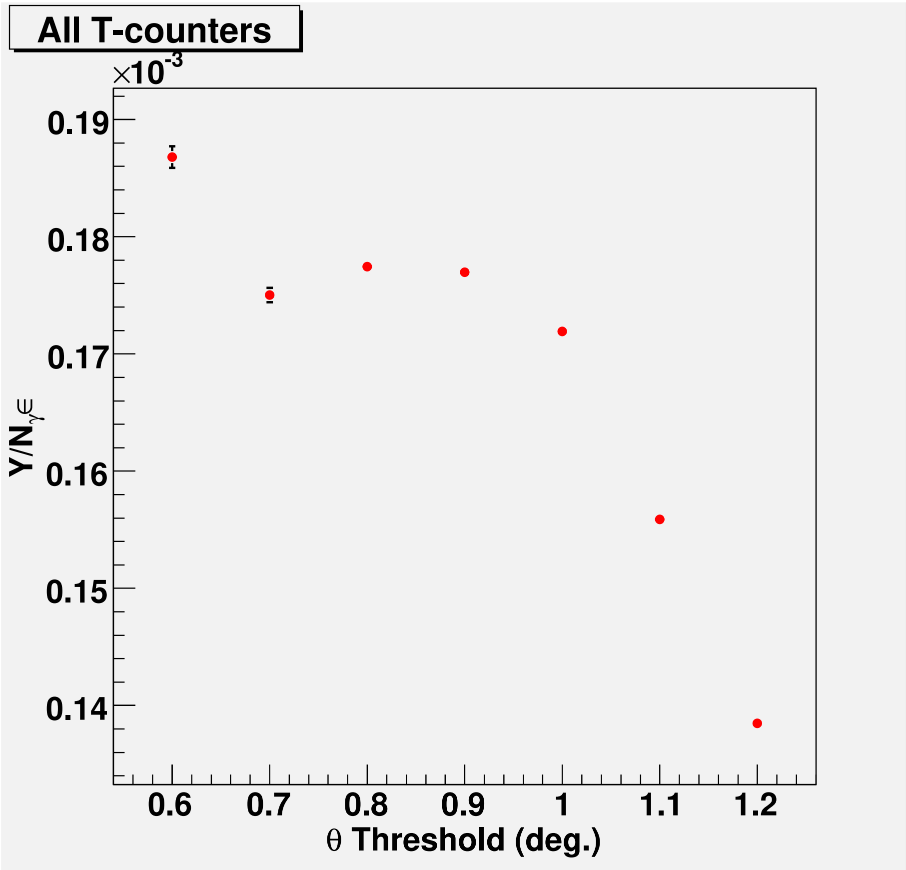

Figure 21: Normalized yield as a function of θ_{max} for a π^0 production run. The normalized yield begins to plateau at $\theta_{max} = 0.9°$. The θ_{min} is fixed at $0.5°$.

The fact that $\theta_{max} > 0.9°$ is the onset of the trigger inefficiency is confirmed by the theory. Eq. 1 has been used to calculate the scattered photon energy over a given θ range for an incident photon energy of 5.5 GeV. Fig. 22 shows the scattered photon energy versus θ. At $\theta = 0.9°$, the scattered photon energy is approximately 2 GeV which is the trigger threshold for the π^0 production runs. Clearly, there is a trigger inefficiency which is lowering the measured cross section for the π^0 production data. Unfortunately, this results show in the previous section incorporated the cut of $\theta_{max} = 0.9°$. The source of the remaining inefficiency is not known well enough at this time to correct the results.

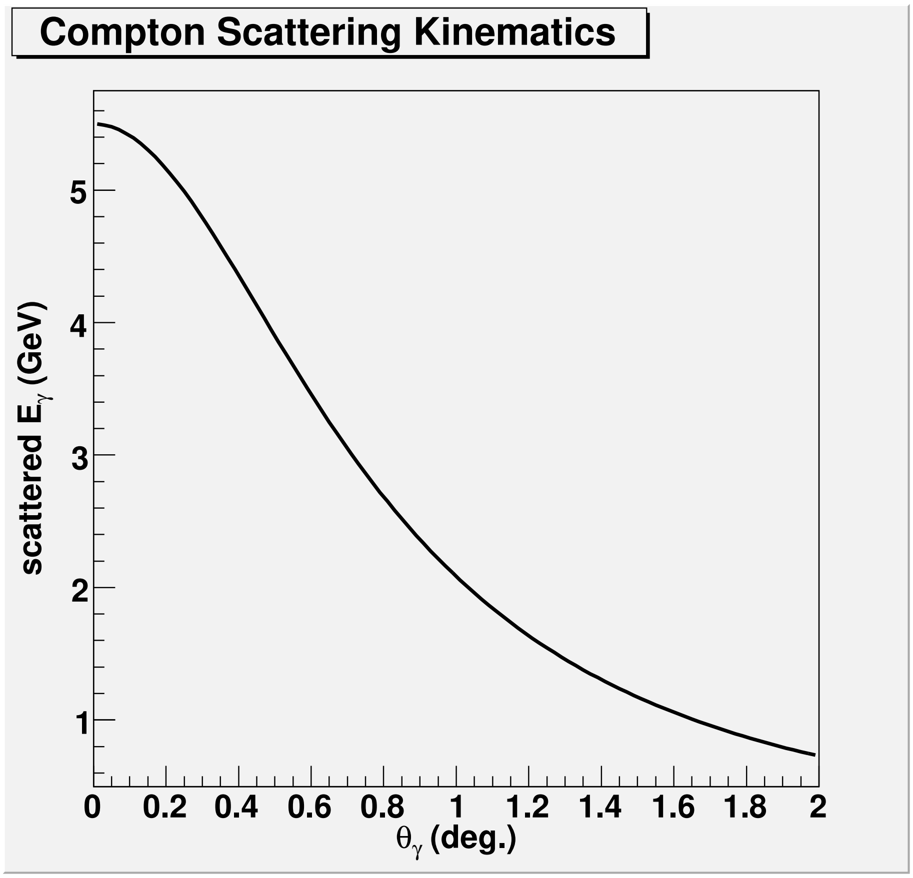

Figure 22: Theoretical calculation of the scattered photon energy versus θ for an incident photon energy of 5.5 GeV. At $\theta = 0.9°$, the scattered photon energy is approximately 2 GeV which corresponds to the hardware threshold for π^0 production runs.

7 Stability Studies

Even though the trigger inefficiency does not allow for an absolute cross section measurement, the relative cross section can be utilized as a monitor for beam and detector stability. The cross section has been determined for most of the π^0 production runs with the carbon target and radiator B. By plotting the cross section versus run number, the data should be constant, and any points which are outside of the errors can be investigated. Since the target and acceptance should not change, the stability check will indicate a change in yield (HyCal problems) or photon flux (tagger problems). Fig. 23 shows the relative cross section over many runs. These runs

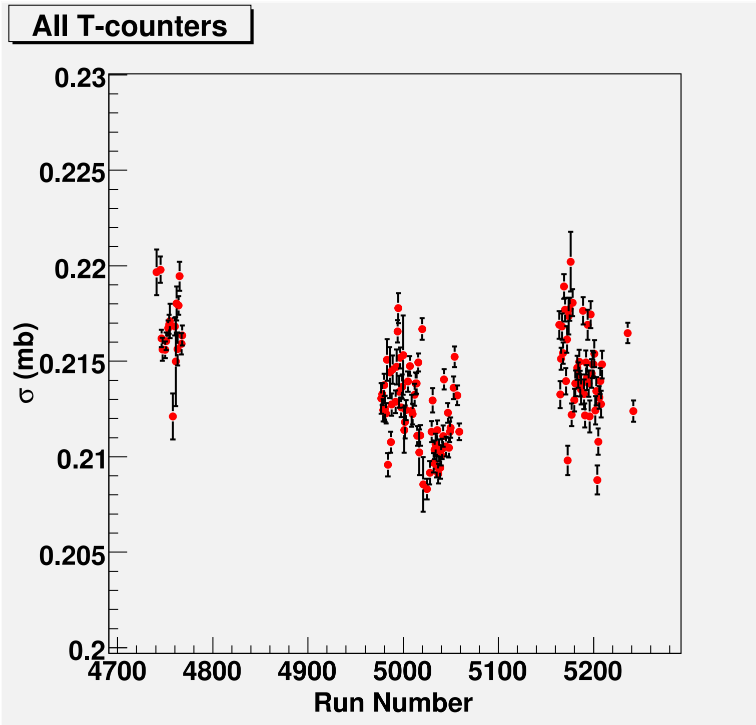

Figure 23: Plots of the relative Compton cross section by run number. The runs encompass the π^0 production runs on a carbon target with photon radiator B.

are divided naturally into three run ranges: 4740-4768, 4976-5068, and 5159-5242. The data show good agreement within each run range. There is an unusual feature that run range 1 is lower than the other ranges.

To quantify this study further, two methods have been applied to guage the point-point variation in each run range. The first method is to project the data in each run range onto the y-axis and fit each distribution with a Gaussian function. The mean from the fit will give a number to the amount of change between each run range. The sigma will give the amount of spread in the data in each range. Fig. 24 shows the Gaussian fits to each distribution. For run range 1, the statistics is small so the weighted mean and RMS have been calculated to compare with the fit parameters. Table 5 lists the results from method 1. The weighted means and

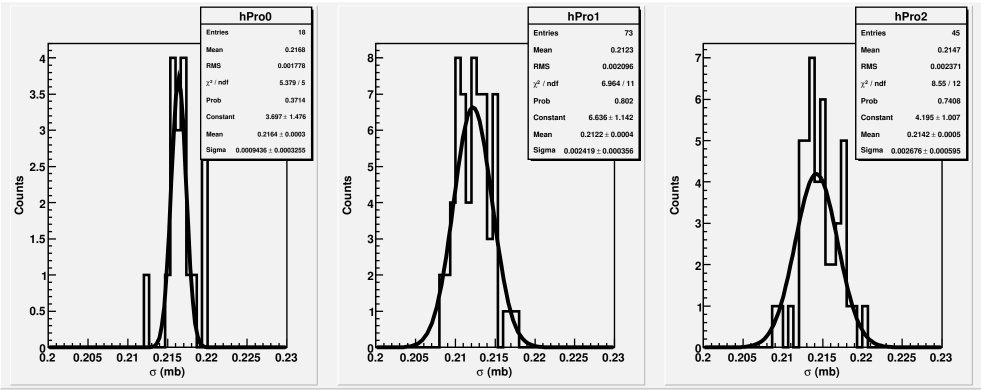

Figure 24: Gaussian fits to the distribution of cross section measurements for a group of runs for stability method 1. The run ranges are labeled 1 (left), 2 (middle), and 3 (right).

fitted means agree quite well. The fitted sigma and RMS are in good agreement and

Table 5: Results of stability method 1.

Run Range	Weighted Mean	RMS	Fitted Mean	Fitted σ
1	0.2168	1.8×10^{-3}	0.2164 ± 0.0003	$9.4 \times 10^{-4} \pm 3.3 \times 10^{-4}$
2	0.2123	2.1×10^{-3}	0.2122 ± 0.0004	$2.4 \times 10^{-3} \pm 3.5 \times 10^{-4}$
3	0.2147	2.4×10^{-3}	0.2142 ± 0.0005	$2.7 \times 10^{-3} \pm 6.0 \times 10^{-4}$

indicate a 1% deviation from the mean. The mean values also show good agreement between the three run ranges.

Method 2 is to fit each run range with a flat line and calculate the χ^2_{ndf}. This method does not address the change in the mean value of each run range but the amount of spread within each range. Fig. 25 contains the fits for each run range. Table 6 lists the χ^2_{ndf} for each fit. The first run range has the smallest number of runs and the least point-to-point variations.

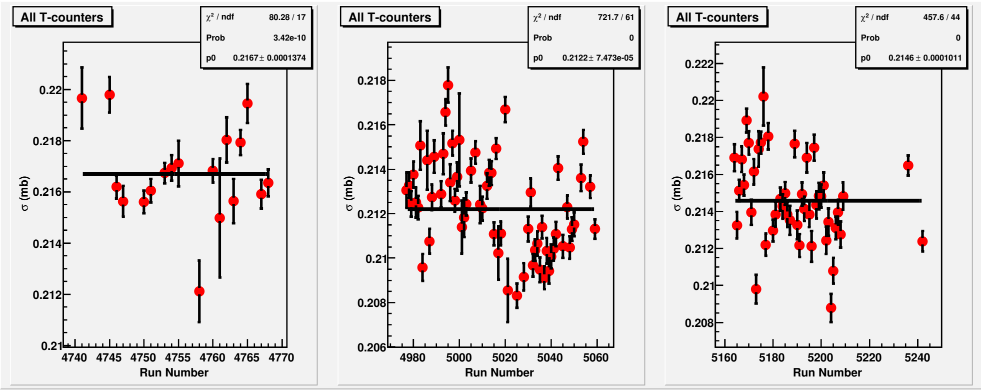

Figure 25: Fits to the distribution of cross section measurements for a group of runs for stability method 2. The run ranges are labeled 1 (left), 2 (middle), and 3 (right).

Table 6: Results χ^2_{ndf} of stability method 2.

Run Range	χ^2	ndf	χ^2_{ndf}
1	80.3	17	4.72
2	722	61	11.8
3	458	44	10.4

Up to this point, the stability has been tested per run range and integrating over all T-counters. The stability has also been studied over T-counters and integrating over all runs. Fig. 26 shows the means and RMS's for each T-counter. From the RMS plots, the results are stable over all T-counters. Fig. 27 shows the χ^2_{ndf} for each T-counter from method 2.

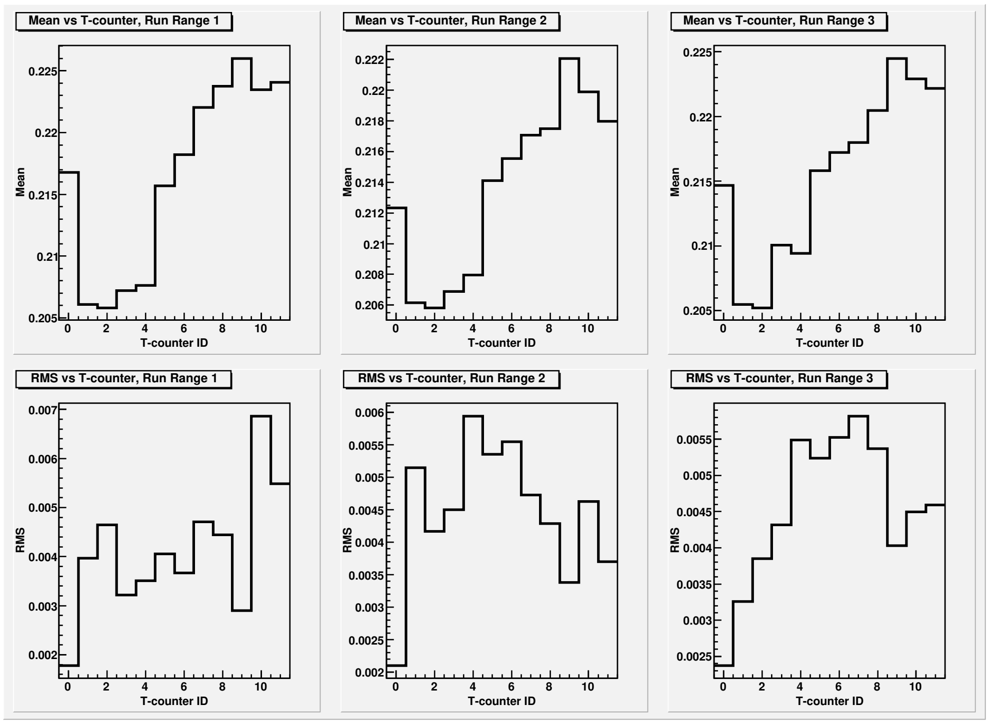

Figure 26: The means (top row) and sigmas (bottom row) per T-counter from the stability method 1. The run ranges are labeled 1 (left), 2 (middle), and 3 (right).

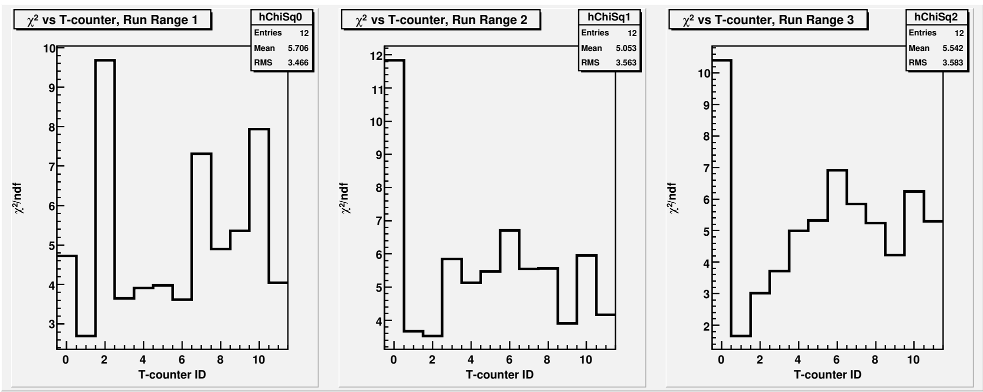

Figure 27: The χ^2_{ndf} per T-counter from the stability method 2. The run ranges are labeled 1 (left), 2 (middle), and 3 (right).

8 Conclusions

In this report, a Compton scattering analysis has been studied by detecting only the scattered photon. This channel is a good choice for systematic checks of the photon flux and detector stability. With a single data run, a statistical accuracy of 1-2% can be obtained. It has been utilized to test for bad data by comparing the relative cross section for π^0 production runs withe the carbon target. With the current analysis, the absolute cross section can be determined with an accuracy of approximately 10% due to trigger inefficiency.

Even though an absolute cross section has not been achieved with an adequate accuracy to aid in the π^0 analyses, a number of recommendations can be made for a second experiment. The first recommendation is to eliminate the trigger inefficiency, an additional prescaled trigger should be included with a hardware threshold set identical to the dedicated Compton scattering runs. With precise knowledge of the prescale factor, the absolute cross section can be measured. The second recommendation is to study the systematic error in the yield extraction. In this report, a 10% difference in yield has been obtained when 2^{nd}-order polynomial, 3^{rd}-order polynomial, and gaussian functions were fit to the background with the data from the π^0 production runs. The background peaks at $R \approx 0.6$ and increases in magnitude as θ decreases. This background most likely is accidental photons scttered from the beamline. The third recommendation is to study the cross section versus θ. In this report, a single angular bin from $0.5°$ to $0.9°$ was used, and the cross section was calculated for each T-counter. Another analysis can be made for different angular bins and integrating over T-counters (incident photon energy).

The single-arm Compton scattering analysis holds great promise. The data has high statistics and is present in the π^0 production runs. The angular range does not extend beyond the $PbWO_4$ region. However, by eliminating the trigger inefficiency, the angular range can extend out beyond $1.5°$ unlike the current analysis with makes a cut at $\theta_{max} = 0.9°$.

The author would like to acknowledge Rory Miskimen for his constant direction and motivation of this analysis. Also, many thanks to David Lawrence and Eric Clinton their advice and borrowed code.

References

[1] P. Martel and R. Miskimen, *Analysis of Primex Targets*, (Primex Note 28), (2004)

[2] Y. Prok, Analysis Note v2,
http://www.jlab.org/primex/secure/yprok_comp_v2_mar09_2007.pdf, (2007).